ACS NANO Cite This: ACS Nano XXXX, XXX, XXX–XXX www.acsnano.org

ARTICLE

Intermittency of Deformation and the Elastic Limit of an Icosahedral Virus under Compression

Mercedes Hernando-Pérez,[†] Cheng Zeng,[‡,§] M. Carmen Miguel,[*,‡] and Bogdan Dragnea[*,¶]

[†]Centro Nacional de Biotecnologia (CNB-CSIC), Darwin, 3, 28049 Madrid, Spain

[‡]Departament de Física de la Matèria Condensada, Facultat de Física, Universitat de Barcelona, Martí i Franquès 1, 08028 Barcelona, Spain

[§]Harvard, John A. Paulson School of Applied Sciences, 29 Oxford Street Cambridge, Massachusetts 02138, United States

[¶]Department of Chemistry, Indiana University, Bloomington, Indiana 47405, United States

Supporting Information

ABSTRACT: **Viruses undergo mesoscopic morphological changes as they interact with host interfaces and in response to chemical cues. The dynamics of these changes, over the entire temporal range relevant to virus processes, are unclear. Here, we report on creep compliance experiments on a small icosahedral virus under uniaxial constant stress. We find that even at small stresses, well below the yielding point and generally thought to induce a Hookean response, strain continues to develop in time *via* sparse, randomly distributed, relatively rapid plastic events. The intermittent character of mechanical compliance only appears above a loading threshold, similar to situations encountered in granular flows and the plastic deformation of crystalline solids. The threshold load is much smaller for the empty capsids of the brome mosaic virus than for the wild-type virions. The difference highlights the involvement of RNA in stabilizing the assembly interface. Numerical simulations of spherical crystal deformation suggest intermittency is mediated by lattice defect dynamics and identify the type of compression-induced defect that nucleates the transition to plasticity.**

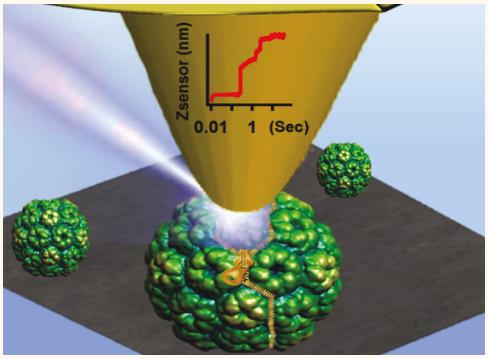

KEYWORDS: *virus, plasticity, atomic force microscopy, nanoindentation*

Symmetric virus shells are natural examples of spherical crystallography.[1−3] Influenced by a topology that necessarily includes intrinsic defects,[4] the dynamic properties of spherical crystals are in many ways distinct from those of crystals in flat space.[5,6] For instance, in three-dimensional metals, the unrestricted length of dislocations gives rise to malleability, a property associated with plastic deformability.[7] However, on a spherical manifold, dislocations have lengths and, presumably mobilities, which are constrained by the curvature of the space they inhabit.[8] Since topological defects hold an important role in the mechanisms of deformation, plastic deformability is expected to be different in spherical crystals from flat space crystals.

In viruses, a proteinaceous closed shell formed from tens to thousands of proteins carries a central role in transport, protection, and delivery of the viral genome. Virus shells may have global or local symmetry only, as in the case of small icosahedral plant viruses[9] or as in some lentiviruses in immature form,[10] respectively. Because of geometrical frustration, that is, the inability of local symmetry to propagate, symmetric shells that are topologically equivalent to a sphere necessarily possess intrinsic defects.[4] In other words, not all constituent subunits can have the same topology. Unlike shells with local symmetry only, where extrinsic defects are present and defect location is stochastic, in symmetric shells intrinsic defect location is deterministic. For instance, in icosahedral shells, 12 disclinations are located at the vertices of the icosahedron.[11]

Involvement of intrinsic defects in the static mechanical properties of viruses is an active area of research.[12−14] While plasticity has been observed in virus particles,[15,16] little is known about the involvement of defect-mediated dynamics in virus deformation. Because of the obvious structural similarities, it is not unreasonable to seek guidance in this sense in the predictions of computational studies of quasi-

Received: March 18, 2019
Accepted: June 25, 2019
Published: June 25, 2019

   DOI: 10.1021/acsnano.9b02133
ACS Nano XXXX, XXX, XXX–XXX

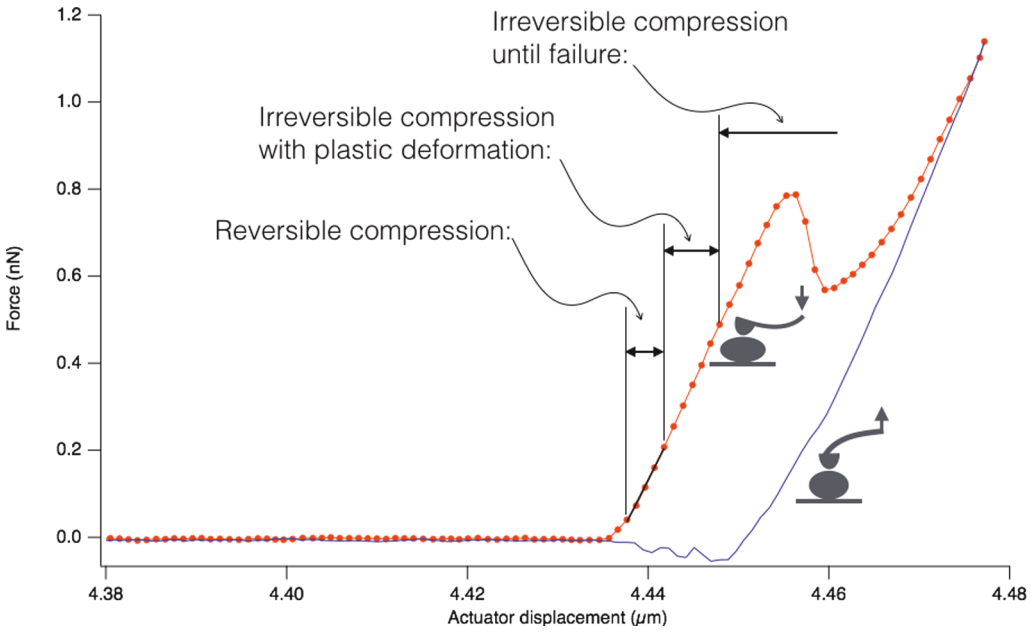

Figure 1. Typical force−displacement curve obtained by AFM on a single brome mosaic virus (BMV) particle adsorbed on mica, showing the indentation force (obtained from cantilever deflection) *versus* *z* piezoactuator displacement. Orange: Compression. Blue: Retraction. A Hooke law fit is shown of the small stress region usually attributed to the elastic regime. The black vertical lines delimit different mechanical regimes. Their locations correspond approximately to values predicted by the coarse-graining simulation of Krishnamani *et al.*[32]

statically deformed curved crystalline shells formed of isotropic particles.[17] Such studies have pointed to the involvement of geometrically necessary disclinations in the collective reorganization of the shell under mechanical stress.[17] Disclinations are aided in the deformation process by the proliferation of dislocation pairs.[17]

Since many virus coats are nearly ideal examples of curved crystalline shells, the question arises whether related dynamics might underlie virus deformation pathways, at sufficiently long time scales. Understanding virus deformation pathways will help in forming a mechanistic view of how virus particles may respond by contact compliance[18] to interactions with the variety of interfaces of the host cell.[19] Identifying processes responsible for virus shell malleability could thus unveil core regulatory principles for biological phenomena, such as virus maturation, endocytosis, or translocation across organelle boundaries.[20−23]

In recent years, nanoindentation by atomic force microscopy (AFM) has been the experimental method of choice for investigating virus shell mechanics *in situ*.[15,22,24−28] In this approach, after having identified the location of a virus on a surface by AFM imaging, the probe is brought in contact with the virus apex. The probe then continuously compresses the virus in a sequence of discrete advancing steps, until a prescribed maximum force is attained at which point the tip is retracted. At each step on the tip−surface approach trajectory, the piezoactuator displacement and the force on the AFM cantilever (which also serves as strain sensor) are recorded. Since the elastic constant of the cantilever can be easily found prior to the experiment by the thermal noise method,[29] virus indentation can be inferred at each step.

Figure 1 presents a typical force−displacement dependence obtained from a single brome mosaic virus particle (BMV) adsorbed on mica, in low ionic strength, low pH buffer, where the virus is most stable. At small indentations, we distinguish a first regime corresponding to a linear response. In this regime, the particle recovers almost entirely at decompression.[30] At the other end of the curve, there is the catastrophic failure regime, where extended plastic events percolate throughout the shell. Here the particle abruptly yields to compression and does not recover during decompression. The limit between these two extremes is not clear. On a similar virus, Michel *et al.* determined that catastrophic failure occurs at indentations between 20% and 30% of the virus diameter and between 0.6 nN and 1.0 nN. Coarse-grained molecular dynamics computations[31,32] suggest that the two limiting cases are separated by a transition regime in which local plastic events start to occur in the molecular network, but most of the initial stiffness is preserved. In this second regime, there is at least partial recovery at decompression.

Phenomenological parameters such as an effective elastic constant (regime I) and the yield force (regime III) can be thus obtained, and have provided the means for direct comparisons of mechanical properties between different virus states. For instance, we now know how different are the stiffnesses of empty capsids *versus* wild-type virions,[30] the effects of specific coat protein mutations on yield force and stiffness,[26,30] the role played by nucleic acid−protein interface in the mechanical stability of the virus,[28,33] and the mechanical behavior in response to chemical cues,[34] and maturation.[22,35,36]

Coarse grained molecular dynamics and multiscale simulations of nanomechanical indentation have provided an increasingly complex picture for the mechanism of virus deformation under uniaxial compression.[12,31,37−40] However, the dynamic range of molecular simulation methods remains limited with respect to the time span of virus dynamics, which extends to minutes. Time-resolved experiments with an expanded dynamic range (from submicroseconds to minutes) are, therefore, required because they provide access to dynamics in a regime yet inaccessible to detailed molecular simulations.

DOI: 10.1021/acsnano.9b02133
ACS Nano XXXX, XXX, XXX−XXX

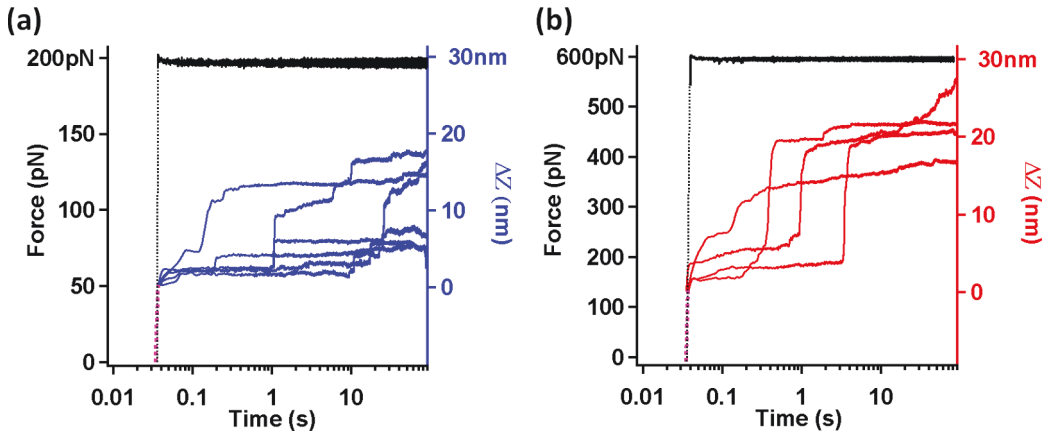

Figure 2. Under constant load, empty BMV capsids and wt BMV undergo a sequence of discrete drops in height (right scale: ΔZ is the *z*-piezo actuator displacement). (a) Empty capsids. Load: 200 pN. Black: Force loading *vs* time. Pink: Initial, rapid *z* piezoextension period. (b) Same experimental variables, but for wtBMV. Load: 600 pN.

In bulk matter, increasing the stress eventually leads to local dissipative and irreversible deformations. The macroscopic description resulting from averaging over these local processes, is the realm of continuum theory of elasticity.[41] One can also average the results of virus AFM indentation among many particles, and describe the average behavior in the language of theory of elasticity.[16,25,31,42,43] However, as noted above, because of the inherent topological defects in the ground state, virus mechanical properties may vary in ways that have no counterpart for bulk matter in flat space. These single-particle specific dynamics could be lost by averaging. Thus, viruses interact with cells individually, in ways that may be qualitatively different from the average behavior. One example is the sequence of contact mechanics events that trigger virus entry, which would be lost by averaging.[44−46] Another example concerns the putative boundary of the elastic regime in single-particle indentation experiments, which will be examined here.

Multiscale computational modeling by Krishnamani *et al.*[32] addressed modalities of failure of virus capsids under stress, at molecular level, and led to three predictions:

1. The computed reversible compression range for the chlorotic cowpea mosaic virus, which is closely related to the brome mosaic virus (BMV) studied here, spanned from 0 to 3 nm. This is a much shorter range than the range of apparent linear stress−strain, Figure 1.
2. The irreversible compression regime was predicted to start well-within the linear portion of the experimental stress−strain curve.
3. Finally, Krishnamani *et al.* predicted that the occurrence of a low threshold for the elastic-to-plastic transition is related to the nucleation of a rupture event at a hexameric interface, that is, there is a well-defined molecular event initiating irreversible deformation, which requires a minimal energy barrier to be overcome by compression work.

We note that, while it is usually assumed that the linearity of the stress−strain relationship warrants reversibility and a Hookean description, in polymer glasses with spatial and dynamic heterogeneity, a linear strain−stress relationship has been observed, even when local plastic events did occur for stresses well below the yield point.[47] Moreover, "fatigue" experiments[48,49] support the idea that such stochastic, plastic local events may also occur, at very small stresses, in viruses. Indeed, this type of experiments have been carried out on different viruses, typically by repeatedly compressing the virus at peak forces of only ∼100 pN. Such repeated small compressions resulted in slow, irreversible transformations, which would be hard to reconcile with a purely elastic material.[16] When added to the predictions of Krishnamani *et al.*, these experimental observations suggest that the dynamics of icosahedral virus shells under compression might also include stochastic plastic events very early on the stress−strain curve. Inspired by the lessons learned from the plasticity of molecular networks encountered in polymer glasses, where dynamic heterogeneity spans a very broad scale, we have decided to expand the time scale over which the dynamics of virus deformation is typically investigated in conventional indentation. To this end, we have performed single virus particle "creep compliance" (Figure SI-1) experiments, with AFM. The data cover a time span from 10^{-3} to 10^{2} s.

These extended dynamic range experiments allowed us to find that, for a small icosahedral virus under constant uniaxial load, strain continues to develop in discrete, relatively sparse jumps, long after the prescribed stress value was attained, and even at small uniaxial loads generally considered to induce a Hookean response. We examine the rheology of a simple icosahedral virus throughout the range of linear behavior, and we show that the intermittent character of the stress−strain curve appears above a load threshold, similar to situations encountered in granular flows, and the plastic deformation of crystalline solids,[50] and in qualitative agreement with prediction 3 of Krishnamani *et al.* Numerical simulations of shells formed of discrete subunits allowed the observation of propagating fractures and highlight the role played by defects in the emergence of intermittency under directional load.

The mechanism for the deformation and failure processes at nanometer length scales in curved crystalline shells, which we hypothesize might operate in viruses too, is thought to consist of an intermittent series of elastic, reversible deformations interrupted by sudden inelastic, plastic events.[17] Since differences between elastic and plastic regimes are most straightforward to observe in time-course experiments, we adopted the creep-compliance approach—a time-resolved technique widely employed for characterization of continuous media[51] but not yet applied to the study of virus mechanics. In creep-compliance experiments, a prescribed stress value is rapidly applied and the strain evolution is recorded in time

DOI: 10.1021/acsnano.9b02133
ACS Nano XXXX, XXX, XXX−XXX

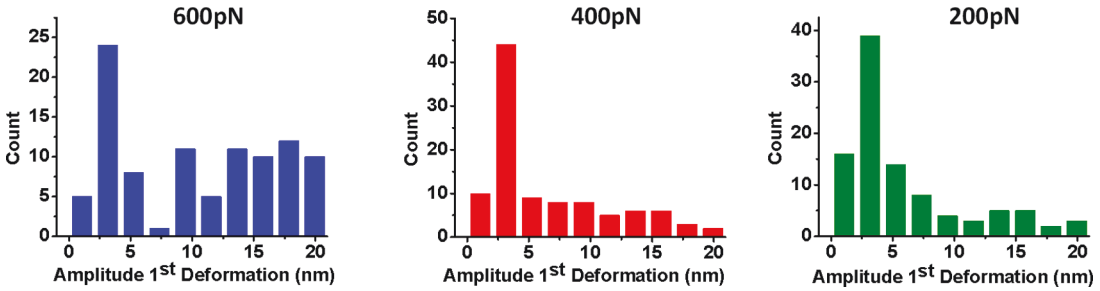

Figure 3. Histograms of the amplitude of first jump leading to creep in compressed BMV (left and center; blue and red, respectively) and empty BMV capsids (right; green).

under constant loading, Figure SI-1. This allows applying the stress in less than 1 ms and following the strain as a function of time over a few minutes, at several kHz sampling rates.

To understand why here we favor the creep compliance approach to the conventional load ramp one,[25] it is useful to point our attention to the Figure 1, where the putative intermittent events are conspicuously absent. Three reasons contribute to their absence: (a) They might be removed by averaging across a population of particles or taken for high-frequency noise and smoothed out (as it was done on the specific data set that produced Figure 1). (b) In conventional nanoindentation experiments, where the loading increases monotonically, any sudden changes in the sample height are convoluted with the probe motion. (The latter is usually in the range 0.5−5 μm/s.) Sudden jumps can thus be undersampled and hard to distinguish from driven probe motion. (c) Because such events are stochastic, not enough time is allowed for their observation in the span of a compression scan (contact time during a scan is typically tens of milliseconds). Since these issues are easy to avoid in the creep-compliance method, we have applied it to study how strain develops in single particles of brome mosaic virus (BMV) in solution, as a function of time, under constant load, for a total set of 341 viral particles: 241 virions and 100 empty particles (see Supporting Information for more experimental details). Note, however, that manifestations of intermittent jumps could also be observed, although over a reduced temporal window, in many of the conventional load ramp curves, see, for example, refs 48, 52, and 53. Since creep compliance experiments can take longer than conventional load ramp experiments precautionary measures have to be taken to avoid thermal drift artifacts (see SI-Methods and Figure SI-3).

RESULTS AND DISCUSSION

Figure 2 presents typical creep data acquired from empty BMV capsids and wild-type (wt) BMV. The prescribed force load in both cases was well below the yield force, which is ∼800 pN for BMV[28,54] (Figure 1), and it was attained in ≲35 ms. Both samples show creep manifesting as a sequence of discrete drops in particle height. Such intermittency can be easily observed after the load has reached its prescribed value. Since intermittent behavior is observed in both types of particles, we deduce that it is a feature of the capsid, and likely due to the discrete nature of its structural subunits.

AFM imaging of the particles before and after completion of creep experiments indicate that, when creep is observed, particle deformation is plastic, that is, permanent at least over the time scale of the experiment (several minutes), Figure SI-2. This is consistent with previous observations by continuous indentation on other icosahedral viruses.[31] Figure SI-2 also shows that virus particles do not change location as a result of compression: after indentation, they occupy the same position and they show signs of irreversible deformation, that is, dimples and cracks, if and only if the force is high enough, in agreement with previous load ramping experiments on similar viruses.[30] This excludes rolling as a potential artifact.

Intermittent jumps and resulting creep was not observed in wild-type virions at any point during a dwell time of ∼90 s for forces below 250 ± 50 pN, Figure SI-2, and for all loading rates we have looked at. In these conditions, the change in height remains constant in time and proportional to the load, as one would expect from an elastic body. Note that, for BMV, the change in height under a 200 pN load is ≲1 nm.[28,54] This truly elastic response at very small loads is consistent with molecular dynamics simulations on the southern bean mosaic virus, which found that the first phase in virus deformation is a Hookean regime resulting from reversible outer surface atom rearrangements,[55] and with the multiscale simulations on CCMV capsids.[32] However, compliance experiments on empty capsids could not detect a similar measurable force threshold separating elastic from intermittent deformation. In this case, we have observed intermittent jumps at every load above the noise floor. If there is a force threshold for empty BMV capsids, it must be below our measurement detection limit, that is, about 4 times less than the force threshold found for BMV. These difference between creep in empty capsids and virions have possible biological implications. Thus, since for such small forces it is reasonable to assume that the compressive stress field does not reach the depth at which RNA is located (≳5 nm below the virus surface), the qualitative difference observed in the elastic threshold between BMV and its empty capsid highlights the involvement of RNA-coat protein interactions in the assembly interface, suggestive of allostery and similar to other viruses.[56]

Histograms of the amplitude of the first deformation jump (from 199 virions and 100 empty capsids) at force loads above the intermittency threshold, show a distinct peak at ∼3 nm, Figure 3. (Note that virions below intermittency threshold were not included in these first jump statistics.) In agreement with prediction 3 of ref 32, we deduce that the onset of intermittent deformation regime is marked by a discrete event, presumably the creation of a certain type of virus shell lattice defect.

Upon examination of particle heights before and after compression by forces greater than ∼0.3 nN, if the force is kept on for a time longer than ∼1s, smaller heights are frequently observed. This is consistent with the results shown in Figure SI-2. However, if the compression is kept less than about 0.1 s, we do not observe differences between the initial and the final

DOI: 10.1021/acsnano.9b02133
ACS Nano XXXX, XXX, XXX−XXX

average height. This is not contradictory with the proposed onset of plastic events because, even if sparse defects that associate with plasticity have appeared in the molecular network, it is not unreasonable that the remaining elastic network might have enough stored elastic energy to restore the overall shape. However, the recovery elastic force will be somewhat different from the initial one (before the local event to occur).

Note that the individual plastic events occur at a rate between 3 and 12 μm/s. These velocities were calculated from the slope of the first jump. These rates are for the most, higher than the typical programmed displacement rates used in conventional AFM indentation.[25] This suggests that, at least for viruses similar to BMV, there are dissipation channels above the elastic threshold that are much faster than the typical loading rate.

The BMV creep compliance characteristics highlighted above bear resemblance with those encountered in soft materials with microscopic spatial heterogeneity,[47] and also in the mechanical deformation of microscopic crystals.[57] Notably, in the latter case, deformation is often characterized by the existence of a well-defined "yield point" below which the crystal response is elastic, and above which plastic deformation is mediated by the collective dynamics of topological defects such as dislocations and grain boundaries.[50] Thus, in small-scale crystals, the transition from elastic to plastic deformation departs from the conventional macroscopic *continuous* description. Stress−strain curves exhibit abrupt jumps or avalanches, either strain bursts or sudden stress drops depending on the deformation protocol, as a result of dislocation activity.[58] Several avalanches intermittently appear whenever irreversible deformation processes, such as those triggered by the nucleation/annihilation of a pair of opposite-sign dislocations, occur even at small loads.

Studies of deformation of curved colloidal crystal shells have indicated that the motion of crystal disclinations, embodied by pentamers in virus capsids, can only occur through the assistance of dislocations, pairs of 5- and 7-fold near-neighbor coordinated sites that attach to an existing disclination.[17] In equilibrium conditions, that is, when the free energy is minimum, the disclination arrangement is correlated with the distribution of Gaussian curvature. After mechanical deformation, the local curvature distribution changes and so the disclination distribution will tend to evolve to accommodate to the new mechanical conditions. According to these findings, strain relaxation will only occur after new dislocations can be nucleated in the crystal. This explains the need of attaining a force threshold above, which the nucleation of a pair of opposite sign dislocations can accommodate the heterogeneous distribution of internal stress in the crystal.

To illustrate in further detail the underlying microstructural changes that can be happening in a simple model for the virus capsids, we performed simulations of dynamic rearrangements of isotropic particles on the surface of a sphere which progressively transformed into an oblate spheroid, while preserving the volume. This minimalistic model is arguably the simplest model that, as we shall see, illustrates behavior dominated by the existence of intrinsic defects which result from geometric frustration.

We start from an initial low energy configuration containing $N = 92$ particles interacting via a Lennard-Jones potential (see Supporting Information). This low-energy configuration contains $N_t = 180$ triangles, that is, the same number of triangles as proteins in the BMV viral capsid, arranged in the form of hexamers and pentamers as in the BMV capsid. The N particles are, thus, confined to the surface of a sphere of radius $R = 14$ nm that we deform quasi-statically into an oblate ellipsoid with time-dependent radial and axial dimensions $R(t)$ and $h(t)$, respectively, as we illustrate in Figure 4. The initial

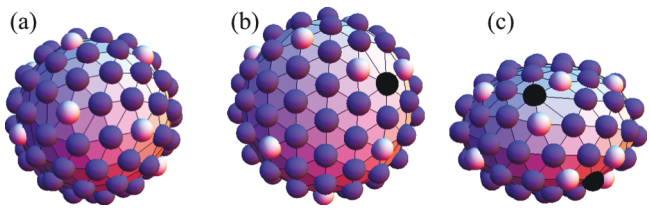

Figure 4. Illustration of simulation geometry (a) before and (b, c) after compression: (b) top view and (c) side view. Blue beads are 6-fold coordinated, black are 7-fold, and white are 5-fold. A few new dislocations, neighboring 7−5-fold bead pairs, remain in the crystal after deformation.

relaxed configuration has icosahedral symmetry with exactly 12 geometrically necessary 5-fold disclinations present. Compression of the spherical structure is done at constant deformation rates.

Dynamics under this mode of deformation is very heterogeneous and exhibits activity bursts similar to those observed previously for bigger colloidal crystals (see Figure SI-4).[17] Simulated stress−strain curves (Figure SI-4) show an initial elastic regime, followed by a few intermittent stress drops that appear in correspondence with velocity bursts, a typical feature of plastic deformation in micron-scale crystals.[17,57,59,60] In conventional geometries, where curvature is not a relevant ingredient, sudden jumps of the stress under either stress or strain-controlled compression tests are known to be due to collective irreversible rearrangements of topological defects, such as dislocations and grain boundaries. Here, despite the small size of the crystals considered, we can also identify a few peaks corresponding to nucleation of new dislocations to dislocation motion and annihilations. Moreover, we observe a reasonable amount of variability and fluctuations in both the elastic and the plastic responses of the crystal structure depending on the relative orientation of the spherical crystal and the deformation axis.

The effective dislocation motion can only occur through the assistance of new dislocations, which enables the growth of grain boundary scars.[17] The nucleation of new dislocations can also accommodate some of the elastic stress that built up with the pressing process. Plastic events first occur intermittently releasing part of this internal stress. As an example, in Figure SI-4, we show a detailed microstructure evolution corresponding to a single plastic burst. The snapshots illustrate a specific defect structure and disclination displacements, which take place through the nucleation of new dislocation dipoles, followed by a dislocation gliding step (Figure SI-5). Defect dynamics preserves at all times the total disclination charge required by Gaussian curvature. The remaining disclinations have, as a result, changed their position on the crystal, as well as their relative orientation. Eventually, at high deformations, small cavities could develop at the edge of the oblate ellipsoid. This cavitation at the edge of the shell changes the topological characteristics of the crystal and dislocation nucleation and flow turns out to be crucial for the annihilation of any excess disclination charge according to the new topology features. It is

DOI: 10.1021/acsnano.9b02133
ACS Nano XXXX, XXX, XXX−XXX

interesting to note that cavities at the edge of the virus shell can be often observed after compression (Figure SI-2).

To determine whether the statistics of activity bursts (jumps) in the experimental data has similarities with that of the model, we measure the distribution of burst magnitudes, defined as the area under each root-mean-square velocity pulse (see Figure SI-3). This is done in practice by defining a small threshold v_{th} and considering as a pulse any sequence of time-points, where the mean-square velocity $\langle |v| \rangle > v_{th}$. The burst magnitude is defined as

$$s_{model} \equiv \int_{t_1}^{t_2} dt \langle |v(t)| \rangle \quad (1)$$

where the times t_1 and t_2 are the times where the pulse starts and ends, respectively. The distribution of avalanche sizes is reported in Figure 5 for a driving rate $v_d = 0.01 v_0$, where v_0 is

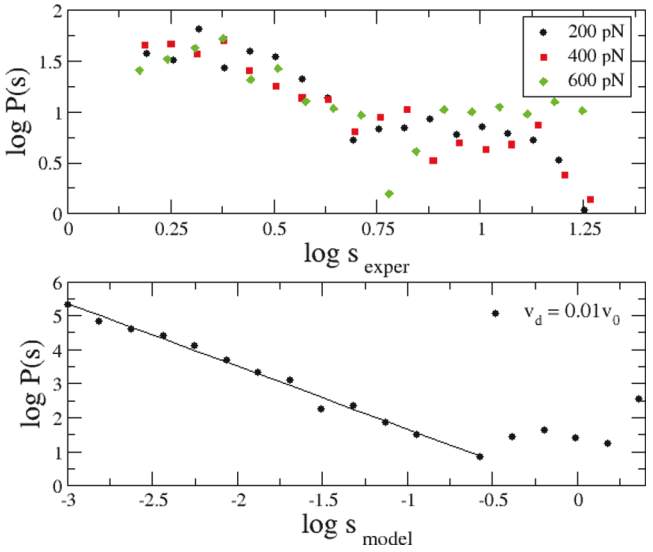

Figure 5. Distribution of activity burst magnitudes in experimental (top) and model (bottom) creep data.

the natural velocity unit in the simulations. The threshold v_{th} has to be larger than the velocity background due to numerical noise, but small enough to record the signal. In the present case, a good choice is $v_{th} = 10^{-3} v_0$.

Although the limited sample size and the lack of experimental bursts statistics does not allow a detailed analysis, the plots are qualitatively similar. Specifically, they exhibit a power law characteristic with exponent values between 1.5 and 2.0, for both experimental and simulation distributions. It is interesting to see that such a simple model predicts a scaling law that has similarities with the one exhibited by the experiment and, furthermore, that it agrees with the findings of some of the more sophisticated multiscale coarse-grained simulations, which have predicted an early elastic-to-plastic transition nucleated in the vicinity of topological defects. In view of the simplicity of the model, the exact nature of such nucleation event for the elastic to plastic transition should be further tested by both experiment and theory. Nevertheless, the results support the view that the same statistical framework that creates a coarse-grained description of dislocation response may be useful in bridging the gap between the behavior of individual defects and the ensemble of dislocations that presumably govern mesoscopic virus plasticity.

CONCLUSION

In conclusion, we have shown that the mechanical deformation built up in a small BMV icosahedral virus under uniaxial constant stress continues to develop intermittently in time long after a fast initial load was applied. This striking response is only observed above a given threshold load. While the value of this threshold is small (<300 pN) suggesting a local nucleation event, it depends on the presence of RNA. We posit that, above a critical stress, virus deformation dynamics is constituted of a sequence of viscoplastic events, sparsely distributed in time, similar to those observed in crystal plasticity at small scales. Simulations of a curved crystalline particle shell with the number of subunits as BMV corroborate that the interplay of several topological defects could be responsible for the intermittent plasticity observed in the real virus. Specifically, local topological defect rearrangements, involving dislocation nucleation and dislocation-disclination reactions, allow geometrically necessary disclinations to change their spatial distribution and relative orientations triggering plastic events, or plastic avalanches. This viscoplastic response allows the system to partially release the mechanical tension accumulated in the nanocrystalline structure, as in other, more conventional materials.

Our work highlights the importance of topological defects in the dynamics of virus shells under mechanical stress beyond the elastic regime and could stimulate further experiments needed to deepen our understanding of nonequilibrium phenomena in curved crystals, as well as ideas about the physical mechanisms by which viruses and viruslike particles cope with the mechanical stresses that ensue at different stages of virus life-cycle.

METHODS/EXPERIMENTAL SECTION

Sample Preparation. Purification of BMV was done following the protocols in ref 61. Briefly, BMV was expressed in *Nicotiana benthamiana* plants *via Agrobacterium*-mediated gene delivery. The leaves were collected 7 days post infection and stored at −80 °C until use. The leaves were first homogenized in virus buffer [250 mM NaOAc, 10 mM $MgCl_2$, pH 4.5] and then centrifuged at 5000 rpm for 25 min at 5 °C on a Beckman TA-10.250 rotor to remove undissolved materials. The supernatant was then layered on a 10% sucrose cushion (w/v) in virus buffer and centrifuged at 26 000 rpm for 3 h on a Beckman SW 32 rotor. The pellets were resuspended in 38.5% CsCl (w/v) in virus buffer and centrifuged at 45 000 rpm for 24 h on a Beckman Ti-70.1 rotor. The virus band was then collected and dialyzed, with three changes in 24 h, against SAMA buffer (50 mM NaOAc, 8 mM $Mg(OAc)_2$, pH 4.5). Final purity of wild-type virus was achieved by running the virus on a Superos-6 column by fast protein liquid chromatography (FPLC). The purified virus was stored under −80 °C until use.

Atomic Force Microscopy. All AFM experiments were conducted with a Cypher AFM (Asylum Research, Santa Barbara, U.S.A.) in liquid. A stock solution of purified BMV was diluted in SAMA buffer (pH 4.5) into a final concentration of 0.1 mg/mL prior each AFM experiment. A single droplet (50 μL) of diluted virus sample was deposited on a freshly cleaved highly oriented pyrolytic graphite (HOPG, ZYB quality, NT-MDT) and incubated for at least 20 min. Excess solution was then blotted away with filter paper, and the sample was washed three times with buffer to remove loose particles. We have used gold-coated, soft silicon nitride microcantilevers BioLever Mini (Olympus, Tokyo, Japan) with a nominal spring constant of ~0.09 N/m and rectangular tips with 9 ± 2 nm radii of curvature for imaging and indentation. Prewetting of tips was done with a drop (~40 μL) of the SAMA buffer. AFM images were acquired in intermittent, AC mode. The cantilever spring constant

DOI: 10.1021/acsnano.9b02133
ACS Nano XXXX, XXX, XXX−XXX

and quality factor of the first flexural mode was calibrated using the thermal noise method.[29]

For creep experiments, the viral particle was centered in the scan area and the AFM tip was positioned on the top. After ramping compression to a prescribed load, the probe was kept under constant loading forces over a dwell time of 90 s. More details on AFM measurement, statistics and representative AFM images are available in the Supporting Information.

ASSOCIATED CONTENT

Supporting Information

The Supporting Information is available free of charge on the ACS Publications website at DOI: 10.1021/acsnano.9b02133.

Details on experimental (AFM, sample preparation) and computational procedures and supplemental figures supporting the main text (PDF)

AUTHOR INFORMATION

Corresponding Authors

*E-mail: carmen.miguel@ub.edu.
*E-mail: dragnea@indiana.edu.

ORCID

Mercedes Hernando-Pérez: 0000-0002-5875-5620
Bogdan Dragnea: 0000-0003-0611-2006

Notes

The authors declare no competing financial interest.

ACKNOWLEDGMENTS

B.D. acknowledges insightful discussions at the Aspen Physics Center with William S. Klug, who pointed out that the experiments we were doing were known as "creep-compliance tests", in mechanical engineering. The work was supported by the Army Research Office, under award W911NF-17-1-0329, and by the National Science Foundation, under award CBET 1740432. M.C.M. acknowledges financial support from the Spanish Government's MINECO under project FIS2016-76830-C2-2-P.

REFERENCES

(1) Tarnai, T.; Gáspár, Z. Multi-Symmetric Close Packings of Equal Spheres on the Spherical Surface. *Acta Crystallogr., Sect. A: Found. Crystallogr.* **1987**, *43*, 612−616.
(2) Lidmar, J.; Mirny, L.; Nelson, D. R. Virus Shapes and Buckling Transitions in Spherical Shells. *Phys. Rev. E* **2003**, *68*, 51910.
(3) Bowick, M. J.; Nelson, D. R.; Shin, H. Interstitial Fractionalization and Spherical Crystallography. *Phys. Chem. Chem. Phys.* **2007**, *9*, 6304−6312.
(4) Sadoc, J.-F.; Mosseri, R. *Geometrical Frustration*; Cambridge University Press: Cambridge, 2006.
(5) Wales, D. J. Chemistry, Geometry, and Defects in Two Dimensions. *ACS Nano* **2014**, *8*, 1081−5.
(6) Guerra, R. E.; Kelleher, C. P.; Hollingsworth, A. D.; Chaikin, P. M. Freezing on a Sphere. *Nature* **2018**, *554*, 346−350.
(7) Phillips, R. *Crystals, Defects and Microstructures: Modeling Across Scales*; Cambridge University Press: Cambridge, 2001.
(8) Bausch, A. R.; Bowick, M. J.; Cacciuto, A.; Dinsmore, A. D.; Hsu, M. F.; Nelson, D. R.; Nikolaides, M. G.; Travesset, A.; Weitz, D. A. Grain Boundary Scars and Spherical Crystallography. *Science* **2003**, *299*, 1716−1718.
(9) Casjens, S. *Virus Structure and Assembly*; Jones & Bartlett Pub.: Boston, 1985.
(10) Mateu, M. G., Ed. *Structure and Physics of Viruses—An Integrated Textbook*; Springer Subcellular Biochemistry; Springer: Dordrecht, the Netherlands, 2013; Vol. *68*.
(11) Caspar, D. L.; Klug, A. Physical Principles in the Construction of Regular Viruses. *Cold Spring Harbor Symp. Quant. Biol.* **1962**, *27*, 1−24.
(12) Zandi, R.; Reguera, D. Mechanical Properties of Viral Capsids. *Phys. Rev. E* **2005**, *72*, 021917.
(13) Cartagena, A.; Hernando-Pérez, M.; Carrascosa, J. L.; de Pablo, P. J.; Raman, A. Mapping *In Vitro* Local Material Properties of Intact and Disrupted Virions at High Resolution Using Multi-Harmonic Atomic Force Microscopy. *Nanoscale* **2013**, *5*, 4729.
(14) Klug, W. S.; Roos, W. H.; Wuite, G. J. L. Unlocking Internal Prestress from Protein Nanoshells. *Phys. Rev. Lett.* **2012**, *109*, 168104.
(15) Ivanovska, I. L.; de Pablo, P. J.; Ibarra, B.; Sgalari, G.; MacKintosh, F. C.; Carrascosa, J. L.; Schmidt, C. F.; Wuite, G. J. L. Bacteriophage Capsids: Tough Nanoshells with Complex Elastic Properties. *Proc. Natl. Acad. Sci. U. S. A.* **2004**, *101*, 7600−5.
(16) de Pablo, P. J.; Mateu, M. G. Mechanical Properties of Viruses. *Subcell. Biochem.* **2013**, *68*, 519−51.
(17) Negri, C.; Sellerio, A. L.; Zapperi, S.; Miguel, M. C. Deformation and Failure of Curved Colloidal Crystal Shells. *Proc. Natl. Acad. Sci. U. S. A.* **2015**, *112*, 14545−14550.
(18) Zeng, C.; Hernando-Pérez, M.; Dragnea, B.; Ma, X.; van der Schoot, P.; Zandi, R. Contact Mechanics of a Small Icosahedral Virus. *Phys. Rev. Lett.* **2017**, *119*, 038102.
(19) Barrow, E.; Nicola, A. V.; Liu, J. Multiscale Perspectives of Virus Entry *via* Endocytosis. *Virol. J.* **2013**, *10*, 177.
(20) Sun, S. X.; Wirtz, D. Mechanics of Enveloped Virus Entry into Host Cells. *Biophys. J.* **2006**, *90*, L10−2.
(21) Veesler, D.; Johnson, J. E. Virus Maturation. *Annu. Rev. Biophys.* **2012**, *41*, 473−496.
(22) Pang, H.-B.; Hevroni, L.; Kol, N.; Eckert, D. M.; Tsvitov, M.; Kay, M. S.; Rousso, I. Virion Stiffness Regulates Immature HIV-1 Entry. *Retrovirology* **2013**, *10*, 4.
(23) Greber, U. F. Virus and Host Mechanics Support Membrane Penetration and Cell Entry. *J. Virol.* **2016**, *90*, 3802−3805.
(24) Roos, W. H.; Gibbons, M. M.; Arkhipov, A.; Uetrecht, C.; Watts, N. R.; Wingfield, P. T.; Steven, A. C.; Heck, A. J. R.; Schulten, K.; Klug, W. S.; Wuite, G. J. L. Squeezing Protein Shells: How Continuum Elastic Models, Molecular Dynamics Simulations, and Experiments Coalesce at the Nanoscale. *Biophys. J.* **2010**, *99*, 1175−1181.
(25) Roos, W. H.; Bruinsma, R.; Wuite, G. J. L. Physical Virology. *Nat. Phys.* **2010**, *6*, 733−743.
(26) Castellanos, M.; Pérez, R.; Carrasco, C.; Hernando-Pérez, M.; Gómez-Herrero, J.; de Pablo, P. J.; Mateu, M. G. Mechanical Elasticity as a Physical Signature of Conformational Dynamics in a Virus Particle. *Proc. Natl. Acad. Sci. U. S. A.* **2012**, *109*, 12028−33.
(27) Mateu, M. G. Mechanical Properties of Viruses Analyzed by Atomic Force Microscopy: A Virological Perspective. *Virus Res.* **2012**, *168*, 1−22.
(28) Vaughan, R.; Tragesser, B.; Ni, P.; Ma, X.; Dragnea, B.; Kao, C. C. The Tripartite Virions of the Brome Mosaic Virus Have Distinct Physical Properties That Affect the Timing of the Infection Process. *J. Virol.* **2014**, *88*, 6483−6491.
(29) Hutter, J.; Bechhoefer, J. Calibration of Atomic-Force Microscope Tips. *Rev. Sci. Instrum.* **1993**, *64*, 1868−1873.
(30) Michel, J. P.; Ivanovska, I. L.; Gibbons, M. M.; Klug, W. S.; Knobler, C. M.; Wuite, G. J. L.; Schmidt, C. F. Nanoindentation Studies of Full and Empty Viral Capsids and the Effects of Capsid Protein Mutations on Elasticity and Strength. *Proc. Natl. Acad. Sci. U. S. A.* **2006**, *103*, 6184−6189.
(31) Arkhipov, A.; Roos, W. H.; Wuite, G. J. L.; Schulten, K. Elucidating the Mechanism Behind Irreversible Deformation of Viral Capsids. *Biophys. J.* **2009**, *97*, 2061−2069.
(32) Krishnamani, V.; Globisch, C.; Peter, C.; Deserno, M. Breaking a Virus: Identifying Molecular Level Failure Modes of a Viral Capsid by Multiscale Modeling. *Eur. Phys. J. Spec. Top.* **2016**, *225*, 1757.
(33) Snijder, J.; Uetrecht, C.; Rose, R. J.; Sanchez-Eugenia, R.; Marti, G. A.; Agirre, J.; Guérin, D. M. A.; Wuite, G. J. L.; Heck, A. J. R.;

DOI: 10.1021/acsnano.9b02133
ACS Nano XXXX, XXX, XXX−XXX

Roos, W. H. Probing the Biophysical Interplay between a Viral Genome and Its Capsid. *Nat. Chem.* **2013**, *5*, 502−509.
(34) Wilts, B. D.; Schaap, I. A.; Schmidt, C. F. Swelling and Softening of the Cowpea Chlorotic Mottle Virus in Response to pH Shifts. *Biophys. J.* **2015**, *108*, 2541−2549.
(35) Roos, W. H.; Gertsman, I.; May, E. R.; Brooks, C. L.; Johnson, J. E.; Wuite, G. J. L. Mechanics of Bacteriophage Maturation. *Proc. Natl. Acad. Sci. U. S. A.* **2012**, *109*, 2342−2347.
(36) Kol, N.; Shi, Y.; Tsvitov, M.; Barlam, D.; Shneck, R. Z.; Kay, M. S.; Rousso, I. A Stiffness Switch in Human Immunodeficiency Virus. *Biophys. J.* **2007**, *92*, 1777−1783.
(37) May, E. R.; Brooks, C. L. Determination of Viral Capsid Elastic Properties from Equilibrium Thermal Fluctuations. *Phys. Rev. Lett.* **2011**, *106*, 188101.
(38) Tama, F.; Brooks, C. L. Diversity and Identity of Mechanical Properties of Icosahedral Viral Capsids Studied with Elastic Network Normal Mode Analysis. *J. Mol. Biol.* **2005**, *345*, 299−314.
(39) Kononova, O.; Snijder, J.; Brasch, M.; Cornelissen, J.; Dima, R. I.; Marx, K. A.; Wuite, G. J. L.; Roos, W. H.; Barsegov, V. Structural Transitions and Energy Landscape for Cowpea Chlorotic Mottle Virus Capsid Mechanics from Nanomanipulation *In Vitro* and *In Silico*. *Biophys. J.* **2013**, *105*, 1893−903.
(40) Aznar, M.; Roca-Bonet, S.; Reguera, D. Viral Nanomechanics with a Virtual Atomic Force Microscope. *J. Phys.: Condens. Matter* **2018**, *30*, 264001.
(41) Landau, L.; Lifshitz, E. M. *Theory of Elasticity*, 3rd ed.; Elsevier Science: Amsterdam, 1984.
(42) Rayaprolu, V.; Manning, B. M.; Douglas, T.; Bothner, B. Virus Particles as Active Nanomaterials That Can Rapidly Change Their Viscoelastic Properties in Response to Dilute Solutions. *Soft Matter* **2010**, *6*, 5286−5288.
(43) Wang, H.; Wang, X.; Li, T.; Lee, B. Transient Viscoelasticity Study of Tobacco Mosaic Virus/Ba2+ Superlattice. *Nanoscale Res. Lett.* **2014**, *9*, 300.
(44) Rankl, C.; Kienberger, F.; Wildling, L.; Wruss, J.; Gruber, H. J.; Blaas, D.; Hinterdorfer, P. Multiple Receptors Involved in Human Rhinovirus Attachment to Live Cells. *Proc. Natl. Acad. Sci. U. S. A.* **2008**, *105*, 17778−17783.
(45) Sieben, C.; Kappel, C.; Zhu, R.; Wozniak, A.; Rankl, C.; Hinterdorfer, P.; Grubmüller, H.; Herrmann, A. Influenza Virus Binds its Host Cell Using Multiple Dynamic Interactions. *Proc. Natl. Acad. Sci. U. S. A.* **2012**, *109*, 13626−31.
(46) Alsteens, D.; Newton, R.; Schubert, R.; Martinez-Martin, D.; Delguste, M.; Roska, B.; Müller, D. J. Nanomechanical Mapping of First Binding Steps of a Virus to Animal Cells. *Nat. Nanotechnol.* **2017**, *12*, 177−183.
(47) Papakonstantopoulos, G. J.; Riggleman, R. A.; Barrat, J.-L.; de Pablo, J. J. Molecular Plasticity of Polymeric Glasses in the Elastic Regime. *Phys. Rev. E* **2008**, *77*, 041502.
(48) Ortega-Esteban, A.; Condezo, G. N.; Pérez-Berná, A. J.; Chillón, M.; Flint, S. J.; Reguera, D.; San Martín, C.; de Pablo, P. J. Mechanics of Viral Chromatin Reveals the Pressurization of Human Adenovirus. *ACS Nano* **2015**, *9*, 10826−10833.
(49) Hernando-Pérez, M.; Lambert, S.; Nakatani-Webster, E.; Catalano, C. E.; de Pablo, P. J. Cementing Proteins Provide Extra Mechanical Stabilization to Viral Cages. *Nat. Commun.* **2014**, *5*, 4520.
(50) Miguel, M. C., Rubi, M., Eds. *Lecture Notes in Physics: Jamming, Yielding, and Irreversible Deformation in Condensed Matter*; Springer: Heidelberg, 2006.
(51) Fung, Y.-C. *Foundations of Solid Mechanics*; Prentice-Hall: Englewood Cliffs, 1965.
(52) Snijder, J.; Ivanovska, I. L.; Baclayon, M.; Roos, W. H.; Wuite, G. J. L. Probing the Impact of Loading Rate on the Mechanical Properties of Viral Nanoparticles. *Micron* **2012**, *43*, 1343−50.
(53) Roos, W. H.; Wuite, G. J. L. Nanoindentation Studies Reveal Material Properties of Viruses. *Adv. Mater.* **2009**, *21*, 1187−1192.
(54) Hernando-Perez, M.; Zeng, C.; Delalande, L.; Tsvetkova, I. B.; Bousquet, A.; Tayachi-Pigeonnat, M.; Temam, R.; Dragnea, B. Nanoindentation of Isometric Viruses on Deterministically Corrugated Substrates. *J. Phys. Chem. B* **2016**, *120*, 340−347.
(55) Zink, M.; Grubmüller, H. Mechanical Properties of the Icosahedral Shell of Southern Bean Mosaic Virus: A Molecular Dynamics Study. *Biophys. J.* **2009**, *96*, 1350−1363.
(56) Zlotnick, A.; Mukhopadhyay, S. Virus assembly, Allostery and Antivirals. *Trends Microbiol.* **2011**, *19*, 14−23.
(57) Dimiduk, D. M.; Woodward, C.; Lesar, R.; Uchic, M. D. Scale-free Intermittent Flow in Crystal Plasticity. *Science* **2006**, *312*, 1188−90.
(58) Alava, M. J.; Laurson, L.; Zapperi, S. Crackling noise in plasticity. *Eur. Phys. J.: Spec. Top.* **2014**, *223*, 2353−2367.
(59) Greer, J. R.; De Hosson, J. T. Plasticity in Small-sized Metallic Systems: Intrinsic *Versus* Extrinsic Size Effect. *Prog. Mater. Sci.* **2011**, *56*, 654−724.
(60) Friedman, N.; Jennings, A. T.; Tsekenis, G.; Kim, J.-Y.; Tao, M.; Uhl, J. T.; Greer, J. R.; Dahmen, K. A. Statistics of Dislocation Slip Avalanches in Nanosized Single Crystals Show Tuned Critical Behavior Predicted by a Simple Mean Field Model. *Phys. Rev. Lett.* **2012**, *109*, 095507.
(61) Kao, C. C.; Sivakumaran, K. Brome Mosaic Virus, Good for an RNA Virologist's Basic Needs. *Mol. Plant Pathol.* **2000**, *1*, 91−97.

DOI: 10.1021/acsnano.9b02133
ACS Nano XXXX, XXX, XXX−XXX